JOURNAL OF GEOPHYSICAL RESEARCH, VOL. 113, C10002, doi:10.1029/2007JC004579, 2008

Stokes drift–induced and direct wind energy inputs into the Ekman layer within the Antarctic Circumpolar Current

Kejian Wu[1] and Bin Liu[1,2]

Received 6 October 2007; revised 18 June 2008; accepted 17 July 2008; published 4 October 2008.

[1] Theoretical analysis of energetics of the Ekman layer by incorporating the Coriolis-Stokes forcing into the classical Ekman model shows that the wind energy input to the Ekman layer has two components: the work done by the wind stress on the surface Ekman current and that done by the Coriolis-Stokes forcing on the whole body of water in the mixed layer. Under the assumption of constant vertical diffusivity, analytical forms of the direct wind energy input and the Stokes drift–induced energy input are derived. Assessments of relative importance of surface waves are made by comparing the wind energy input into the Ekman layer with and without wave-induced Stokes drift effects included. Using the European Centre for Medium-Range Weather Forecasts 40-year reanalysis wind stress and surface wave data sets, the total rate of wind energy input into the Ekman layer within the Antarctic Circumpolar Current (ACC) is estimated to be 833 GW, in which the direct wind energy input is 650 GW (78%), and the Stokes drift–induced energy input is 183 GW (22%). The total mechanical energy input into the ACC due to wave effects is increased by approximately 4% (30 GW) compared to that into the classical Ekman layer. Long-term variability of direct wind and Stokes drift–induced energy inputs to the ACC is also examined.

Citation: Wu, K., and B. Liu (2008), Stokes drift–induced and direct wind energy inputs into the Ekman layer within the Antarctic Circumpolar Current, *J. Geophys. Res.*, *113*, C10002, doi:10.1029/2007JC004579.

1. Introduction

[2] As a major circulation system of the world ocean circulation, the Antarctic Circumpolar Current (ACC) connects the Pacific, Indian, and Atlantic ocean basins and exchanges water mass, momentum, and energy among them. It has also long been recognized as playing a critical role in climate change [*Rintoul et al.*, 2001]. To maintain the ACC itself and its teleconnection with the ocean basins and the climate variability, the wind energy is the most important mechanical energy source. There have been a number of studies on the ACC through observational, theoretical, and numerical methods in the past several decades. However, most of them focused on the dynamical and thermodynamical balance of the ACC [*Rintoul et al.*, 2001]. Quantitative study of the wind energy input into the ACC is still lacking.

[3] Several authors have studied the energetics of ocean circulation [*Wunsch and Ferrari*, 2004]. Up to the present, we have known that the wind energy input to the geostrophic current, integrated over the world ocean, is estimated as 1 TW [*Wunsch*, 1998]. The global wind energy flux to the Ekman layer is estimated as 0.5–0.7 TW over the near-inertial motions [*Alford*, 2003; *Watanabe and Hibiya*, 2002], and the wind energy input over the subinertial motions is 2.3–2.4 TW [*Wang and Huang*, 2004a]. *Wang and Huang* [2004b] have also estimated the wind energy input into the ocean produced through the surface waves as 60 TW on the basis of an empirical formula and wavefields from ocean wave modeling. It is shown that most of the wind energy input into either the Ekman layer or the surface waves is mostly concentrated within the ACC. However, in *Wang and Huang*'s [2004a, 2004b] studies, wind energy inputs into the Ekman layer and into the surface waves were discussed independently. Within the framework of ocean circulation theory, whether or not the surface waves could influence the wind energy input into the circulation is unclear.

[4] For several reasons, the study on wind energy input to the Ekman layer within the ACC should take the surface wave influences into account. First, the wind work on the Ekman layer depends on both the wind stress and the wind-driven current profile. This current profile in the mixed layer is actually predicted by the classical Ekman model, assuming a balance between the Coriolis force and divergence of momentum transfer by turbulence stress. However, observational evidence did not support the classical Ekman model [*Price and Sundermeyer*, 1999; *Lewis and Belcher*, 2004; *Polton et al.*, 2005]. There are three features that cannot be predicted by the Ekman model.

[5] 1. The surface current lies at an angle of between 10° and 45° to the surface wind stress [*Huang*, 1979].

[1]Physical Oceanography Laboratory, Ocean University of China, Qingdao, China.

[2]Also at Department of Marine, Earth and Atmospheric Sciences, North Carolina State University at Raleigh, Raleigh, North Carolina, USA.

0148-0227/08/2007JC004579$09.00

Cushman-Roisin [1994] documented a smaller angle ranging from 5° to 10°.

[6] 2. At a depth between 5 and 20 m the current is deflected by approximately 75° from the wind stress [*Price and Sundermeyer*, 1999].

[7] 3. The current is rapidly attenuated below the surface [*Price and Sundermeyer*, 1999].

[8] Recent studies show that the surface waves play an important role in determining the wind-driven current profile. By incorporating the wave-induced Coriolis-Stokes forcing into the momentum balance of the classical Ekman layer, the analytical solution is shown to agree reasonably well with current profiles from observations and certainly agrees much better than the classical Ekman model [*Polton et al.*, 2005]. Thus, to estimate the wind energy input into the Ekman layer, surface wave effects cannot be neglected.

[9] Second, *McWilliams and Restrepo* [1999] studied the wave-driven effects on the basin-scale circulation. Their results showed that the wave-driven effects sometimes are significant compared to the wind-driven ones. Particularly in midlatitudes or high latitudes (such as the ACC), where the winds are stronger, the wave-induced Stokes transport is a significant fraction of the Ekman transport. Since both the Stokes and Ekman transports carry the mechanical energy which is from the wind energy produced through the surface waves and the Ekman layer, respectively, we believe that surface waves would also have a substantial impact on the wind energy input into the Ekman layer within the ACC. Fairly recently, *Liu et al.* [2007] estimated the global wind energy input to subinertial motions in the Ekman-Stokes layer, where the surface waves are incorporated. However, details of wind energy input to the Ekman-Stokes layer over the ACC were not discussed.

[10] Finally, as will be discussed in section 2, surface waves will significantly affect the total rate of wind energy input into the Ekman layer when the wave-induced Stokes drift is not in the same direction as the wind stress. Actually, all the past studies on the wave-driven effects on the large-scale motions make the assumption that the wave direction is the same as the wind direction [*Huang*, 1979; *McWilliams and Restrepo*, 1999; *Lewis and Belcher*, 2004; *Polton et al.*, 2005]. As will be shown in section 3 (Figure 7), the time-averaged wave directions predicted from the operational ocean wave model (WAM) have systematic deviations to the wind stress vectors. The existence of the angle between wind stress and the Stokes drift implies that surface waves not only have a substantial impact on the total amount of wind energy input to the Ekman layer but redistribute the wind energy between the direct and indirect wind energy inputs as well. This also motivates us to study the wave influences on the wind energy input into the ACC.

[11] Furthermore, recent studies on the wave effects on the Ekman layer use the empirical formulas to estimate the wave characteristics from wind stress [*Lewis and Belcher*, 2004; *Polton et al.*, 2005]. Obviously, a more accurate estimate of the Stokes drift–induced energy input to the Ekman layer depends on the accurate calculation of the Stokes drift directly from either observations or numerical wave models. Although direct observation of the Stokes drift is not realistic within the ACC, the wavefields from a wave-forecasting model have been available for several decades.

[12] This paper aims to estimate the direct wind and Stokes drift–induced energy inputs to the Ekman layer within the ACC, with an emphasis on how the surface waves could have affected the wind energy input. The goal of this study is to be achieved through a simple wave-affected Ekman model which has already been used by several authors [*McWilliams and Restrepo*, 1999; *Lewis and Belcher*, 2004; *Polton et al.*, 2005]. Our paper is set out as follows. Section 2 describes the energetics of the wave-affected Ekman layer. In section 3 we discuss the relative importance of wave effects on the wind energy input to the Ekman layer. Section 4 discusses the approach to compute the wind energy input to the non-steady-state Ekman layer. Section 5 gives the estimates of direct wind and Stokes drift–induced energy inputs within the ACC on the basis of the European Centre for Medium-Range Weather Forecasts (ECMWF) 40-year reanalysis (ERA-40) wind and wave data sets. Finally, section 6 presents our conclusions and discussion.

2. Energetics of the Ekman-Stokes Layer

2.1. Energy Balance

[13] This study is focused on wind energy input into the wave-filtered Ekman layer in an ocean of deep and unlimited horizontal extent. Concerning the mean motion, we assume that there are no horizontal pressure gradients, horizontal mean velocity gradients, or sea level elevations. Thus, the coupled potential energy term can be neglected. To investigate surface wave effects on the wind energy input into the Ekman layer, we first consider the energy balance of the wave-affected Ekman layer. By incorporating the wave-induced Coriolis-Stokes forcing into the classical Ekman model, the momentum equation describing the non-steady-state, ageostrophic current in the surface layer is [*McWilliams et al.*, 1997; *Lewis and Belcher*, 2004; *Polton et al.*, 2005]

$$\frac{\partial \mathbf{U}}{\partial t} + f\hat{\mathbf{z}} \times (\mathbf{U} + \mathbf{U}_s) = \frac{\partial}{\partial z}\left(A_z \frac{\partial \mathbf{U}}{\partial z}\right), \tag{1}$$

where the coordinate is set on the mean zero water level with z pointing upward, $\mathbf{U} = (u, v)$ is the horizontal current, $\mathbf{U}_s$ is the Stokes drift produced by the surface waves, $\hat{\mathbf{z}}$ is the unit vector directed upward, f is the Coriolis parameter, A_z is the vertical momentum diffusivity, and t is time.

[14] Compared with the classical Ekman model, the momentum balance of a wave-affected Ekman layer includes the wave-induced Coriolis-Stokes forcing, which is expressed as $-f\hat{\mathbf{z}} \times \mathbf{U}_s$. The Coriolis-Stokes forcing can be interpreted as a result of the interaction of the Stokes drift with planetary vorticity, and its physical explanation has been discussed by several authors [*Hasselmann*, 1970; *Xu and Bowen*, 1994; *Polton et al.*, 2005]. Figure 1 schematically illustrates the relationship of directions between a surface wave and the Coriolis-Stokes forcing in the Southern Hemisphere ($f < 0$). Note that the Coriolis-Stokes forcing is directed to 90° left of the wave direction and the direction of wind stress is not necessarily the same as that of waves. Especially under swell condition the angle between wind vector and wave direction could be as much as 180°. For a monochromatic deep water wave with wave

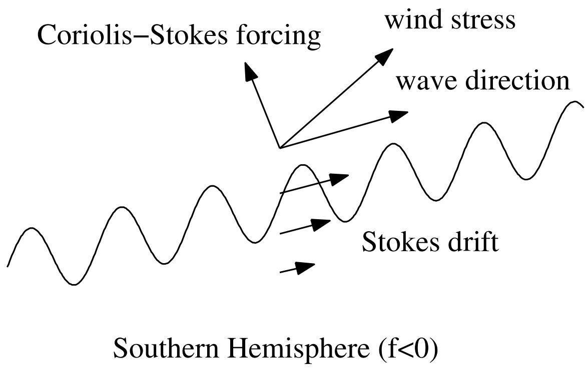

Figure 1. Schematic diagram of the relationship among the directions of wind stress, surface waves, and the wave-induced Coriolis-Stokes forcing in the Southern Hemisphere ($f < 0$).

amplitude a, wave number k, and sea surface wave frequency σ, the Stokes drift profile associated with such a wave is [*Phillips*, 1977]

$$\mathbf{U}_s = U_s e^{2kz}\hat{\mathbf{k}}, \quad U_s = a^2\sigma k, \tag{2}$$

where $\hat{\mathbf{k}}$ is the unit wave number vector and U_s is the velocity of Stokes drift at the sea surface. Note that the Stokes depth scale is $d_s = (1/2k)$, with a typical value of 5–10 m. The Ekman layer including Stokes drift can be called the Ekman-Stokes layer. It satisfies the following boundary conditions:

$$\begin{aligned} &\rho_w A_z \frac{\partial \mathbf{U}}{\partial z} = \boldsymbol{\tau} \quad \text{at } z = 0 \\ &\mathbf{U} \to 0 \text{ as } z \to -\infty, \end{aligned} \tag{3}$$

where ρ_w is water density and $\boldsymbol{\tau}$ is sea surface wind stress. Multiplying equation (1) by $\rho_w\mathbf{U}$ and integrating from $z = -\infty$ to $z = 0$ leads to the energy balance

$$\frac{dE}{dt} = E_w + E_s - D, \tag{4}$$

where

$$\begin{aligned} &E = \rho_w \int_{-\infty}^{0} \frac{1}{2}|\mathbf{U}|^2 dz, \quad E_w = \boldsymbol{\tau}\cdot\mathbf{U}(0), \\ &E_s = \rho_w \int_{-\infty}^{0} (\hat{\mathbf{z}}f \times \mathbf{U}_s)\cdot\mathbf{U}dz, \quad D = \rho_w \int_{-\infty}^{0} A_z\left|\frac{\partial \mathbf{U}}{\partial z}\right|^2 dz \end{aligned} \tag{5}$$

represent the total kinetic energy of the Ekman-Stokes layer, the rate of direct wind energy input, the rate of energy input caused by the Coriolis-Stokes forcing, and the dissipation rate, respectively. Note that the energy input E_w is the work rate done by wind stress acting on the surface Ekman current. Compared to the energy balance of the classical Ekman model [*Wang and Huang*, 2004a], a new term of energy input (E_s) which can be called the Stokes drift–induced energy input, is introduced into the energy balance because of the Coriolis-Stokes forcing. This term can be considered as the work done by the Coriolis-Stokes forcing acting on the per unit horizontal area of a water column in the mixed layer. Since the Coriolis-Stokes forcing originates from the interaction of wind-generated waves with planetary vorticity, the Stokes drift–induced energy input can be considered as a part of indirect wind energy input.

[15] For the steady state Ekman layer, $E_w + E_s = D$; that is, the energy input is balanced by dissipation. In the classical Ekman layer, the wind energy input sustains the turbulence and mixing in the upper ocean; however, in the Ekman-Stokes layer, the energy source of turbulence and mixing should include Stokes drift–induced wind energy input.

2.2. Steady State Solution

[16] If assuming a constant vertical diffusivity and using the complex notation to reexpress the variables $\mathbf{U} = (u, v)$, $\mathbf{U}_s = (u_s, v_s)$, and $\boldsymbol{\tau} = (\tau_x, \tau_y)$ as $\mathbf{U} = u + iv$, $\mathbf{U}_s = u_s + iv_s$, and $\boldsymbol{\tau} = \tau_x + i\tau_y$ respectively, the steady state solution to equation (1) can be easily written as

$$\mathbf{U} = \mathbf{W}_e + \mathbf{W}_{es} + \mathbf{W}_s \tag{6}$$

$$\mathbf{W}_e = \frac{\boldsymbol{\tau}}{\rho_w A_z j}e^{jz}, \quad \mathbf{W}_{es} = -\frac{2kj\mathbf{U}_s(0)}{(2k)^2 - j^2}e^{jz}, \quad \mathbf{W}_s = \frac{j^2\mathbf{U}_s(0)}{(2k)^2 - j^2}e^{2kz}. \tag{7}$$

Here $j = (1 + i)/d$ and $d = \sqrt{2A_z/f}$. Note that equations (6) and (7) are applicable for both the Northern Hemisphere ($f > 0$) and the Southern Hemisphere ($f < 0$). The depth of the Ekman layer d_e is defined as

$$d_e = \sqrt{\frac{2A_z}{|f|}}. \tag{8}$$

Polton et al. [2005] discussed details of the solution to the Ekman-Stokes layer. Note that the first term ($\mathbf{W}_e$) is the classical Ekman solution when the wave-induced effects were not included. However, the second term ($\mathbf{W}_{es}$) and the third term ($\mathbf{W}_s$) are the two new terms introduced by the Coriolis-Stokes forcing. Arising as a particular solution to the Coriolis-Stokes forcing, $\mathbf{W}_s$ decays over the Stokes depth scale d_s. Importantly, there is an Ekman-Stokes component of the current ($\mathbf{W}_{es}$). This term decays over the Ekman depth scale d_e and changes the current profile through the whole depth of the Ekman layer. Since both of these new terms of the solution were introduced by inclusion of the Coriolis-Stokes forcing in equation (1), one has enough reasons to expect that they would have important influences on mechanical energy input to the Ekman-Stokes layer.

2.3. Direct Wind and Stokes Drift–Induced Energy Inputs

[17] From the steady state solution of the Ekman-Stokes layer and after tedious manipulations, the direct wind energy input into the mixed layer can be derived as

$$E_w = E_{w,1} + E_{w,2} + E_{w,3}, \tag{9}$$

where

$$E_{w,1} = \frac{|\boldsymbol{\tau}|^2}{\rho_w d_e |f|}, \quad E_{w,2} = -\boldsymbol{\tau} \cdot \mathbf{U}_s(0) F_1(c),$$
$$E_{w,3} = \pm \hat{\mathbf{z}} \cdot [\boldsymbol{\tau} \times \mathbf{U}_s(0)] F_2(c). \tag{10}$$

The third term ($E_{w,3}$) takes positive sign if $f > 0$ and negative sign if $f < 0$. The two functions F_1 (c) and $F_2(c)$ are expressed as

$$F_1(c) = \frac{c+2}{(c+1)^2+1}, \quad F_2(c) = \frac{c}{(c+1)^2+1}. \tag{11}$$

The nondimensional parameter c is the Ekman-Stokes depth number defined as the ratio of the depth of the Ekman layer to that of the Stokes drift (d_e/d_s), which plays an important role in discussions of the relative importance of wave influences on wind-driven currents [*Weber*, 1983; *Xu and Bowen*, 1994; *McWilliams and Restrepo*, 1999]. We name it the Ekman-Stokes depth number. Apparently, the direct wind energy input to the Ekman-Stokes layer consists of three terms. The first term ($E_{w,1}$) is exactly the wind energy input to the Ekman layer without wave effects included. Details of this energy input associated with its estimate for the world ocean have been discussed recently by *Wang and Huang* [2004a]. The second and third terms ($E_{w,2}$ and $E_{w,3}$), however, are two new terms introduced into the wind energy input by the Coriolis-Stokes forcing. Both of them depend on the Ekman-Stokes depth number, the Stokes drift, and the wind stress vector. The relationship of directions between surface waves and the Coriolis-Stokes forcing in the Southern Hemisphere ($f < 0$) is shown in Figure 1, and the wind stress direction does not necessarily coincide with the wave direction. Notice that if the wind stress is oriented perpendicular to the left (right) of the direction of the Stokes drift in the Southern Hemisphere ($f <$ 0), $E_{w,2}$ will vanish and $E_{w,3}$ will reach its maximum (minimum) value. Such a case would only occur in a swell-dominated area.

[18] There are two limiting cases for $E_{w,2}$ and $E_{w,3}$. First, under the case when the depth of the Ekman layer is much greater than that of the Stokes drift layer ($c \rightarrow \infty$), both $E_{w,2}$ and $E_{w,3}$ tend to zero. This corresponds to a case where influences of Coriolis-Stokes forcing on the Ekman layer vanish, and E_w reduces to wind energy input to the classical Ekman layer $E_{w,1}$. Second, under the case when the Ekman layer depth is much smaller than the Stokes drift depth (c $\rightarrow$ 0), $E_{w,2}$ reduces to $-\boldsymbol{\tau} \cdot \mathbf{U}_s$ (0), and $E_{w,3}$ tends to zero. As pointed out by *Polton et al.* [2005], this case in the ocean might represent swell propagation over a shallow wind-driven layer.

[19] Similarly, the Stokes drift–induced energy input also consists of three terms:

$$E_s = E_{s,1} + E_{s,2} + E_{s,3}, \tag{12}$$

where

$$E_{s,1} = \rho_w |f| d_s |\mathbf{U}_s(0)|^2 F_3(c), \quad E_{s,2} = -E_{w,2}, \quad E_{s,3} = E_{w,3}, \tag{13}$$

and the function $F_3(c)$ is expressed as

$$F_3(c) = \frac{c^2(c^3 - c^2 + 2)}{(c^4+4)\left[(c+1)^2+1\right]}. \tag{14}$$

The second term of the Stokes drift–induced energy input has an opposite magnitude compared to the second term of the direct wind energy input, while the third term is the same as that of the direct wind energy input. $E_{s,2}$ vanishes when $c \rightarrow \infty$ and reduces to $\boldsymbol{\tau} \cdot \mathbf{U}_s$ (0) when $c \rightarrow 0$. Furthermore, for both limiting cases, $E_{s,1} = 0$. Physically, in the real ocean when a swell propagates over a shallow wind-driven layer, the Stokes drift–induced energy input through Coriolis-Stokes forcing will be the work done by the wind stress directly on the surface Stokes drift.

[20] From the expressions of direct wind energy input and Stokes drift–induced energy input discussed above, we can easily obtain the total amount of energy input E_{tot}, so that

$$E_{\text{tot}} = E_{w,1} + E_{s,1} + 2E_{s,3}. \tag{15}$$

In comparison with the wind energy input to the classical Ekman layer ($E_{w,1}$), the total energy input to the Ekman-Stokes layer is increased by $E_{s,1} + 2E_{s,3}$. The reduced part of energy input ($E_{w,2}$) from the direct wind energy input is exactly transferred into $E_{s,2}$ in the Stokes drift–induced energy input through the Coriolis-Stokes forcing. For both cases of $c \rightarrow \infty$ and $c \rightarrow 0$, since $E_{s,1} \rightarrow 0$ and $E_{s,3} \rightarrow 0$, the total amount of energy input tends to the wind energy input into the classical Ekman layer. Thus, whenever $d_e \gg d_s$ or $d_e \ll$ d$_s$, the energy input to the Ekman-Stokes layer by the Coriolis-Stokes forcing can be neglected.

3. Estimates of Stokes Drift–Induced Energy Input

[21] To estimate the relative importance of the direct wind and Stokes drift–induced energy inputs on the basis of equations (9), (13), and (15), four ratios are considered in this study: ratio R_1 of $E_{s,1}$ to $E_{w,1}$, ratio R_2 of $E_{s,2}$ to $E_{w,1}$, ratio R_3 of $E_{s,3}$ to $E_{w,1}$, and ratio R_4 of $E_{s,1} + 2E_{s,3}$ to $E_{w,1}$. We can write them as

$$R_1 = \left[\frac{\rho_w d_s |f| |\mathbf{U}_s(0)|}{|\boldsymbol{\tau}|}\right]^2 c F_3(c), \tag{16}$$

$$R_2 = \frac{\rho_w d_e |f| |\mathbf{U}_s(0)| \cos(\theta)}{|\boldsymbol{\tau}|} F_1(c), \tag{17}$$

$$R_3 = \frac{\rho_w d_e |f| |\mathbf{U}_s(0)| \sin(\theta)}{|\boldsymbol{\tau}|} F_2(c), \tag{18}$$

and $R_4 = R_1 + 2R_3$, respectively, where θ is defined as the angle that the Stokes drift turns to the right of the wind stress vector.

[22] Obviously, ratio R_1 gives how much of the energy input to the Ekman layer increases by inclusion of the Coriolis-Stokes forcing for the case in which the wind stress vector coincides with the Stokes drift (i.e., $\theta = 0°$). Ratio R_2 compares the transferred energy input by the Stokes drift–induced effect $E_{s,2}$ to $E_{w,1}$, presenting how much of the energy input is transferred by the Coriolis-Stokes forcing within the Ekman-Stokes layer. Ratio R_3 gives how much of the energy input to the Ekman layer increases because of the effect of angle θ. Ratio R_4 gives how much of the total energy input increases when including wave effects, compared to the energy input to the classical Ekman layer. We can see that these ratios depend on the magnitudes of both the Stokes drift and wind stress, the nondimensional Ekman-Stokes depth number c, and the angle θ. To further proceed with the estimates of these ratios, we make an assumption that the angle θ is limited within $-90°$ and $90°$.

[23] First, it seems difficult to estimate the depth of the Ekman layer since there are no observations for the vertical diffusivity A_z. Conventionally, the Ekman layer depth is expressed as an empirical formula, $d_e = \gamma u_{*\mathrm{w}}/f$, where $u_{*\mathrm{w}}$ is the turbulent friction velocity in water, traditionally defined by $u_{*\mathrm{w}} = \sqrt{|\boldsymbol{\tau}|/\rho_w}$, and γ is a nondimensional constant. Although a constant of 0.4 is commonly accepted [*Cushman-Roisin*, 1994], a somewhat smaller value of 0.25–0.4 is also recommended under certain oceanic conditions [*Coleman et al.*, 1990; *Price and Sundermeyer*, 1999]. Using six data sets of observations, *Wang and Huang* [2004a] recently suggested a constant of 0.5. In this study, we will use the mean value ($\gamma = 0.38$) of 0.25–0.5 to estimate the Ekman layer depth so that

$$d_e = 0.38 \frac{u_{*a}}{f} \sqrt{\frac{\rho_a}{\rho_w}}, \tag{19}$$

where ρ_a is the density of air and u_{*a} is the friction velocity in air.

[24] Second, the Stokes drift is determined by the characteristics of surface waves. *Komen et al.* [1994] give a series of wave growth equations based on a number of data sets of observations. *Lewis and Belcher* [2004] use such empirical formulas of amplitude a and peak sea surface wave frequency σ, parameterized by wind characteristics, to deduce $|\mathbf{U}_s(0)|$ and k from a fetch-limited or fully developed sea. For simplicity, we assume here that the waves are fully developed. Using the following expressions for a and σ [cf. *Komen et al.*, 1994, equations (6.71a) and (6.71b)],

$$\frac{g^2 a^2}{4u_{*a}^4} = 1.1 \times 10^3, \quad \frac{\sigma u_{*a}}{g} = 2\pi \times 5.6 \times 10^{-3}, \tag{20}$$

we can obtain the estimate of the Stokes drift depth and hence the Coriolis-Stokes depth number so that

$$d_s = \frac{g}{2\sigma^2}, \quad c = \frac{0.76\sigma^2 u_{*a}}{gf} \sqrt{\frac{\rho_a}{\rho_w}}. \tag{21}$$

[25] Finally, the magnitude of the wind stress vector can be expressed in terms of the 10 m wind speed U_{10} and the atmospheric drag coefficient C_D as $|\boldsymbol{\tau}| = \rho_a C_D U_{10}^2$. Since C_D is normally expressed as an empirical function of wind speed U_{10} and the friction velocity u_{*a} is related to C_D by $u_{*a} = \sqrt{C_D}\, U_{10}$, these ratios can be estimated directly from U_{10} combined with the preassumed angle θ.

[26] Figure 2a shows how R_1 increases with wind speed varying from 1 to 25 m/s for four different latitudes: 15°, 30°, 45°, and 60°. We can see that at midlatitude or high-latitude areas and for a moderate wind speed of 10 m/s, the increased energy input induced by wave effects can reach as much as 4–7% in comparison with the wind energy input to the classical Ekman layer. For a higher wind speed like 20 m/s with latitude 60°, this percentage can reach as much as 20%, indicating that the Stokes drift–induced energy input cannot be neglected in discussions of energetics of the surface mixed layer, particularly in the area of the ACC. Figures 2b, 2c, and 2d show the contours of R_2, R_3, and R_4, respectively, changing with wind speed from 1 to 25 m/s and with θ from $-90°$ to 90° (for 45°S latitude). For a fixed wind speed, the transferred energy input between the direct wind energy input and the Stokes drift–induced energy input decreases as θ varies from 0° to 90° or from 0° to $-90°$ and reaches its maximum at 0° (Figure 2b). There would be no energy transfer when the wind stress is perpendicular to the Stokes drift. For the case of $\theta = 0°$, the transferred energy input is much more than the increased energy input due to the wave effects (e.g., for $U_{10} = 15$ m/s, latitude = 45°S, $R_1 = 8\%$, and $R_2 = 36\%$). Figure 2c shows the effects of θ on the Stokes drift–induced energy input. For a fixed wind speed, R_3 decreases as θ varies from $-90°$ to 90°. In the Southern Hemisphere, when the Stokes drift is directed to the right (left) of the wind stress vector, R_3 is positive (negative), indicating that the third terms in both direct wind and Stokes drift–induced energy inputs make positive (negative) contributions to the total energy input. Figure 2d gives the total increased Stokes drift–induced energy input compared to the wind energy input to the classical Ekman layer, including the effects of θ. Apparently, the total increased energy input can be positive or negative, mostly depending on the angle between the Stokes drift and the wind stress vector. We find that the effects of θ play a more important role than $E_{w,1}$ does in the total energy input.

4. Approach to Compute Wind Energy Input to a Non-Steady-State Ekman-Stokes Layer

[27] The analyses in sections 2.2, 2.3, and 3 are limited to a steady state Ekman-Stokes layer. In the real world ocean, the motions in the Ekman-Stokes layer are far from steady state because of the time-varying wind forcing. The following is focused on the energy input to the non-steady-state Ekman-Stokes layer.

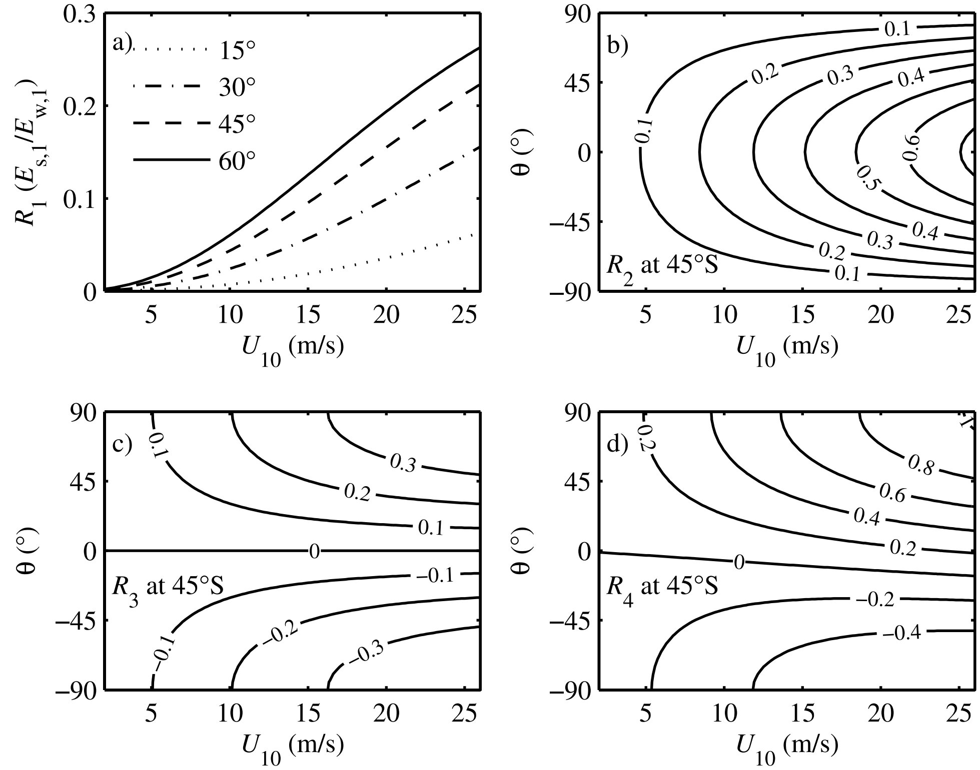

Figure 2. (a) The ratio of $E_{s,1}$ to $E_{w,1}$ (R_1), varying with wind speed U_{10} for four different latitudes: 15°, 30°, 45°, and 60°. (b) The ratio of $E_{s,2}$ to $E_{w,1}(R_2)$, (c) the ratio of $E_{s,3}$ to $E_{w,1}(R_3)$, and (d) the ratio of $E_{s,1}$ + $2E_{s,3}$ to $E_{w,1}$ (R_4), changing with wind speed U_{10} and angle θ between wind vector and wave direction, for 45°S latitude. The θ value is positive when the wave direction is to right of the wind stress direction.

[28] Since we are concerned with wind energy input to the subinertial motions in the Ekman-Stokes layer, the complex variables of current, Stokes drift, and wind stress can be expressed as $\mathbf{U} = \sum_{|\omega_n|<\omega_c} \mathbf{U}_n\, e^{i\omega_n t}$, $\mathbf{U}_s = \sum_{|\omega_n|<\omega_c} \mathbf{X}_n\, e^{i\omega_n t}$, and $\boldsymbol{\tau} = \sum_{|\omega_n|<\omega_c} \mathbf{T}_n\, e^{i\omega_n t}$, with the cutoff frequency ω_c being 0.5 cycle/d. Thus, the nth component of the horizontal momentum equation in the non-steady-state Ekman-Stokes layer can be written as

$$i(f+\omega_n)\mathbf{U}_n + if\mathbf{X}_n = A_z \frac{d^2\mathbf{U}_n}{dz^2}. \tag{22}$$

The corresponding boundary conditions are

$$\begin{aligned} &\rho_w A_z \frac{\partial \mathbf{U}_n}{\partial z} = \mathbf{T}_n \quad \text{at } z=0 \\ &\mathbf{U}_n \to 0 \text{ as } z \to -\infty. \end{aligned} \tag{23}$$

Solving equations (22) and (23) and following the approaches discussed in section 2, we can obtain the direct wind and Stokes drift–induced energy inputs for each of the components.

[29] The direct wind energy input to the non-steady-state Ekman layer for the nth component is

$$E_w^n = E_{w,1}^n + E_{w,2}^n + E_{w,3}^n, \tag{24}$$

where

$$E_{w,1}^n = \frac{|\mathbf{T}_n|^2}{\rho_w d_e^n |f+\omega_n|}, \quad E_{w,2}^n = -\frac{f}{f+\omega_n}[\mathbf{T}_n \cdot \mathbf{X}_n(0)]F_1(c_n),$$
$$E_{w,3}^n = \pm\frac{f}{f+\omega_n}\hat{\mathbf{z}} \cdot [\mathbf{T}_n \times \mathbf{X}_n(0)]F_2(c_n). \tag{25}$$

$E_{w,3}^n$ takes positive sign if $f+\omega_n > 0$ and negative sign if $f+\omega_n < 0$. The Stokes drift–induced energy input for the nth component can be expressed as

$$E_s^n = E_{s,1}^n + E_{s,2}^n + E_{s,3}^n, \tag{26}$$

where

$$E_{s,1}^n = \rho_w \frac{f^2}{|f+\omega_n|} d_s^n |\mathbf{X}_n(0)|^2 F_3(c_n), \quad E_{s,2}^n = -E_{w,2}^n, \quad E_{s,3}^n = E_{w,3}^n. \tag{27}$$

The total energy input to the non-steady-state Ekman layer can be obtained by summing up the energy input for each component:

$$E_{\text{tot}} = \sum_n \left(E_{w,1}^n + E_{s,1}^n + 2E_{s,3}^n\right). \tag{28}$$

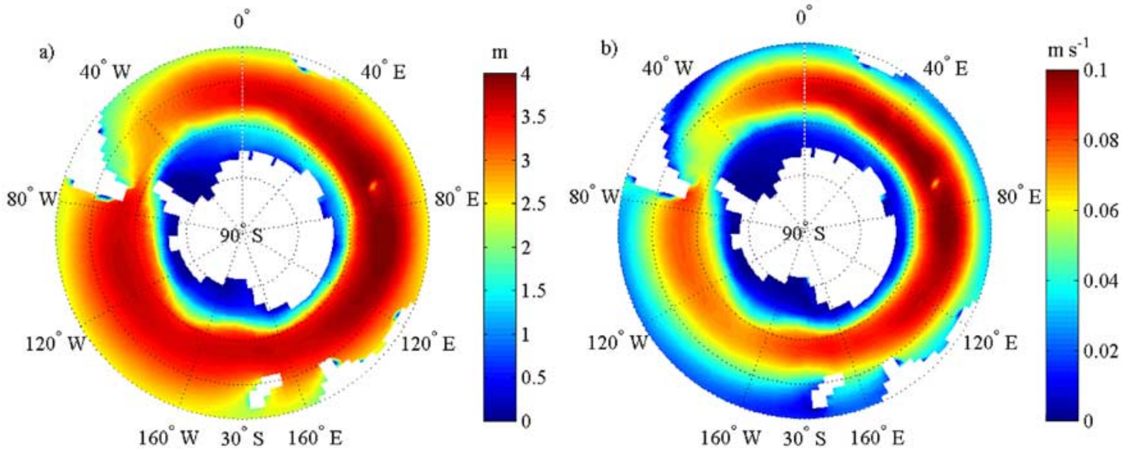

Figure 3. Distributions of the 44-year averaged (a) significant wave height and (b) surface Stokes drift.

Note that d_e^n and c_n are defined for the nth component as

$$d_e^n = \sqrt{\frac{2A_z}{|f + \omega_n|}}, \quad c_n = \frac{d_e^n}{d_s^n} = \frac{d_e}{d_s^n}\sqrt{\frac{|f|}{|f + \omega_n|}}, \qquad (29)$$

respectively, where d_s^n is the nth component of the Stokes depth scale d_s. In the non-steady-state case, we need to consider $f + \omega_n$, instead of f for the steady state case, to compute the direct wind and Stokes drift–induced energy inputs.

5. Results

[30] In this study, we use the ECMWF ERA-40 wind stress and sea surface wave data set to estimate the direct wind and Stokes drift–induced energy inputs into the Ekman layer within the ACC. This data set provides the sea surface wind stress and surface waves predicted from the third-generation WAM. Both the wind stress and surface waves are sampled every 6 h and are regularly gridded with the resolution 2.5° in both the longitudinal and latitudinal directions. This data set covers the period from September 1957 to August 2002. Since the data in 1957 and 2002 are incomplete, we only use the data from 1958 to 2001.

[31] To compute the direct wind and Stokes drift–induced energy inputs, we first calculate the Stokes drift and its depth scale on the basis of the deep water dispersion relation $\sigma^2 = gk$. From the modeled significant wave height H_s and mean wave period T, combined with equation (2), we have

$$U_s = \frac{2\pi^3}{g}\frac{H_s^2}{T^3}, \quad d_s = \frac{gT^2}{8\pi^2}. \qquad (30)$$

The Stokes drift is assumed to be in the same direction as the mean wave direction. Figures 3a and 3b show the 44-year averaged significant wave height and surface Stokes drift near the ACC area, respectively, from which one can see that the averaged surface wave and surface Stokes drift are very strong because of the easterly wind in the ACC area. In order to estimate the contribution to the wind energy input of each component, the complex variable fast Fourier transform is then conducted to the time series of wind stress and Stokes drift at each point with the cutoff frequency ω_c being 0.5 cycle/d. The clockwise- (anticlockwise-) rotating wind stress corresponds to $\omega < 0 (\omega > 0)$, and the steady state component of wind stress corresponds to $\omega = 0$. The Ekman layer depth is computed from equation (19), in which a time-averaged u_{*a} is used.

5.1. Direct Wind and Stokes Drift–Induced Energy Inputs

[32] Using the wind stress and surface wave data set combined with equations (24)–(29), we can compute the direct wind and Stokes drift–induced energy inputs to the Ekman layer for the world ocean. Figures 4a, 4b, 4c, and 4d show the distributions of wind energy input without wave effects included ($E_{w,1}$), wind energy input with wave effects included (E_w), Stokes drift–induced energy input (E_s), and total rate of energy input (E_{tot}), respectively, averaged from 1959 to 2001 in the Southern Ocean (south of 30°S latitude). These distributions are shown to have similar patterns in the three ocean basins, and within the ACC the input is strongest in the Indian Ocean, medium in the Pacific Ocean, and smallest in the Atlantic Ocean. This is because the prevailing westerly winds between about 40° and 60°S generate the strongest Ekman currents and the largest ocean surface waves in the South Indian Ocean, which thus are associated with the strongest direct wind and Stokes drift–induced energy inputs. These energy inputs are also found to be approximately meridional symmetric along 50°S latitude within the ACC. In addition, in the South Atlantic Ocean, particularly the area near the Drake Passage, westerly winds and surface waves are relatively weak because of the continental barrier, and hence, the direct wind and Stokes drift–induced energy inputs are smaller compared to those in other ocean areas.

[33] *Weber* [1983] and *Weber and Melsom* [1993] examine the transfer of momentum to the Ekman layer due to wind and waves and point out that the wave-induced current and the Ekman current at the sea surface could be of the same magnitude. *McWilliams and Restrepo* [1999] conclude that the wave-induced Stokes transport could be comparable with the Ekman transport in high latitudes. Figure 4 shows that the Stokes drift–induced energy input can be on the same order of the direct wind energy input. This confirms

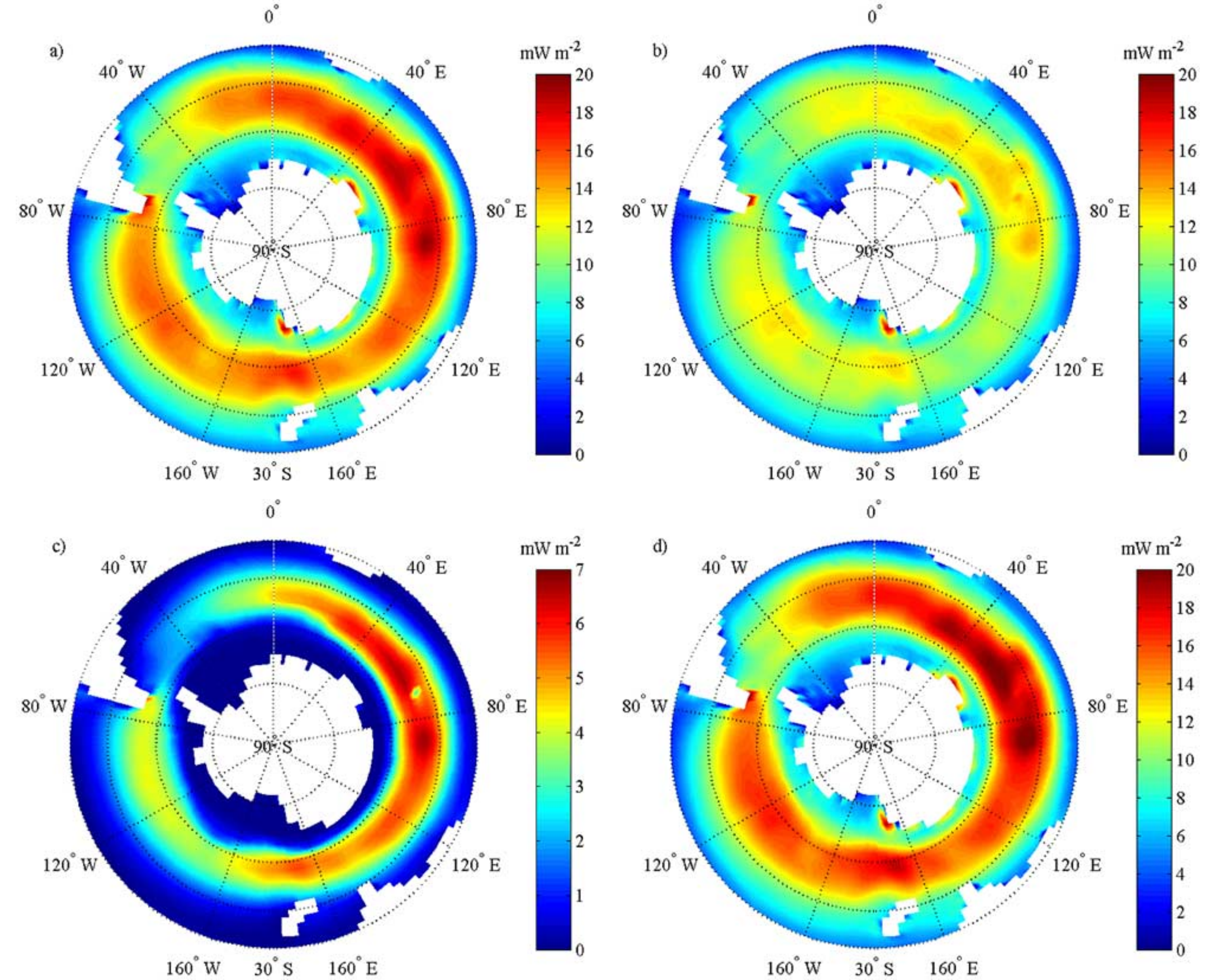

Figure 4. Distributions of direct wind and Stokes drift–induced energy inputs averaged from 1959 to 2001 in the Southern Ocean (south of 30°S latitude): (a) direct wind energy input without wave effects included ($E_{w,1}$); (b) wind energy input with wave effects included (E_w); (c) Stokes drift–induced energy input (E_s); and (d) total rate of wind energy input (E_{tot}).

again the importance of surface waves in the wind energy input to the Ekman layer within the ACC.

[34] In this study, the ACC area is limited from 40° to 60°S. Details of the direct wind and Stokes drift–induced energy inputs, integrated over the ACC, are listed in Table 1. The total rate of wind energy input into the Ekman layer within the ACC is 833 GW, including 650 GW of the direct wind energy input (78%) and 183 GW of the Stokes drift–induced energy input (22%). Compared to the wind energy input to the classical Ekman layer ($E_{w,1}$ = 804 GW), the wind energy input to the Ekman layer with wave effects included is decreased by as much as 154 GW. The total rate of wind energy input, in contrast, is increased by 30 GW, about 4% of the wind energy input to the classical Ekman layer. However, the transferred energy input within the ACC by the Coriolis-Stokes forcing is 144 GW, revealing that about 18% of the wind energy input to the Ekman layer without wave effects was transferred to a part of the work rate done by the Coriolis-Stokes forcing in the Ekman-Stokes layer. From Table 1, one can also find that the main contributions to the wind energy input are from the clockwise- and anticlockwise-rotating wind component. The Stokes drift–induced energy input, however, is mainly from contribution of the steady state wind component.

[35] The meridional distributions of $E_{w,1}$, E$_w$, E_s, and E_{tot}, which are integrated along longitudes within the ACC, are presented in Figure 5a. Figure 5a confirms again the distribution pattern of meridional symmetry along 52°S latitude. Figure 5b gives the zonal distributions of $E_{w,1}$, E_w, E_s, and E_{tot} integrated along latitudes from 40° to 60°S, showing that these energy inputs within the ACC are largest in the Indian Ocean, are coarsely zonal homogeneous in the Pacific, and gradually increase in the South Atlantic away from the Drake Passage to the east.

5.2. Assessment of Wave Influences

[36] To assess wave influences on the wind energy input, Figures 6a–6c present distributions of the three terms in Stokes drift–induced energy input ($E_{s,1}$, $E_{s,2}$, and $E_{s,3}$). The former two terms have similar distribution patterns to those

Table 1. Details of the Direct Wind and Stokes Drift–Induced Energy Inputs Integrated Over the ACC[a]

	$\omega > 0$	$\omega = 0$	$\omega < 0$	Sum
$E_{w,1}$	343.65	238.93	221.06	803.65
$E_{s,1}$	0.05	48.72	0.07	48.84
$E_{s,2}$	1.86	140.90	1.57	144.33
$E_{s,3}$	0.17	−9.50	−0.42	−9.75
E_s	2.09	180.12	1.22	183.42
E_w	341.96	88.54	219.07	649.57
E_{tot}	344.04	268.66	220.29	832.98

[a]All energy input is in GW.

of the wind energy input (Figure 4). It is interesting to note that the distribution of $E_{s,3}$ is distinctively different from those of $E_{s,1}$ and $E_{s,2}$. There is a negative distribution of $E_{s,3}$ near the area along 45°S latitude and a positive distribution near the area approximately along 60°S latitude (Figure 6c), indicating that the surface waves could have positive or negative contributions to the total mechanical energy input. This conclusion is not surprising since the mean wave directions in the above two areas systematically deviate from the wind stress directions (Figure 7). As discussed in section 3, the wave direction turns to the right or left of the wind stress, which determines whether the distributions of $E_{s,3}$ are positive or negative. Most of the great negative distribution of $E_{s,3}$ appears in the Indian Ocean, and the total rate of $E_{s,3}$ integrated over the ACC is about −10 GW. Actually, $E_{s,3}$ distributes very similarly to the near-surface wind pattern: zonally oriented tropical trade winds, midlatitude westerlies, and weak polar easterlies (not shown). The corresponding distribution of $E_{s,3}$ is negative, positive, and negative. This distribution feature can be verified from the averaged wind stress and surface wave directions. The direction of waves turns left, right, and left to that of the wind stress over the corresponding geographical areas, respectively.

5.3. Long-Term Variability of Direct Wind and Stokes Drift–Induced Energy Inputs

[37] Fairly recently, *Huang et al.* [2006] studied the decadal variability of wind energy input to the world ocean. Using the National Centers for Environmental Prediction–National Center for Atmospheric Research wind stress data and ECMWF wind stress data, they found that the wind energy input to the ACC increased 15% over the past 25 years. Because of the great importance of the wind energy input in maintaining the oceanic general circulation, any changes of wind energy input would not only induce changes of barotropic and baroclinic eddy flux but importantly would affect the Ekman transport, which may further influence the meridional overturning circulation in the world ocean. The analysis in sections 5.1 and 5.2 has shown the substantial role that surface waves play in the mechanical energy input to the Ekman layer within the ACC, although the total rate of wind energy input is only increased by approximately 4% compared to that without wave effects included. Nearly 22% of the total energy input is produced through the wave-induced Coriolis-Stokes forcing, indicating that surface waves would also have a substantial impact on the long-term variability of the wind energy input.

[38] Figure 8 presents the yearly variations of $E_{w,1}$, E_w, and E_{tot} integrated over the ACC from 1958 to 2001. Changes and long-term trend of these energy inputs over the past 44 years are clearly shown to be similar to each other. However, there are two quite different trends of the interannual variability before and after 1975. All three energy inputs show a decreasing trend before 1975. After 1975, there is a rapidly increasing trend until 1980, and then these energy inputs show a slightly increasing trend until 2001.

6. Summary and Discussion

[39] In this paper we have sought to examine the direct wind and Stokes drift–induced energy inputs to the Ekman layer within the ACC by incorporation of the wave-induced Coriolis-Stokes forcing into the classical Ekman model. *Lewis and Belcher* [2004] and *Polton et al.* [2005] have recently studied the significant influences of waves on modifying the vertical profile of the Ekman currents. *Wang and Huang* [2004a] have recently estimated the wind energy input to the global oceans by employing the classical Ekman model. In this study we have extended *Wang and Huang*'s [2004a] work to derive analytical forms of direct

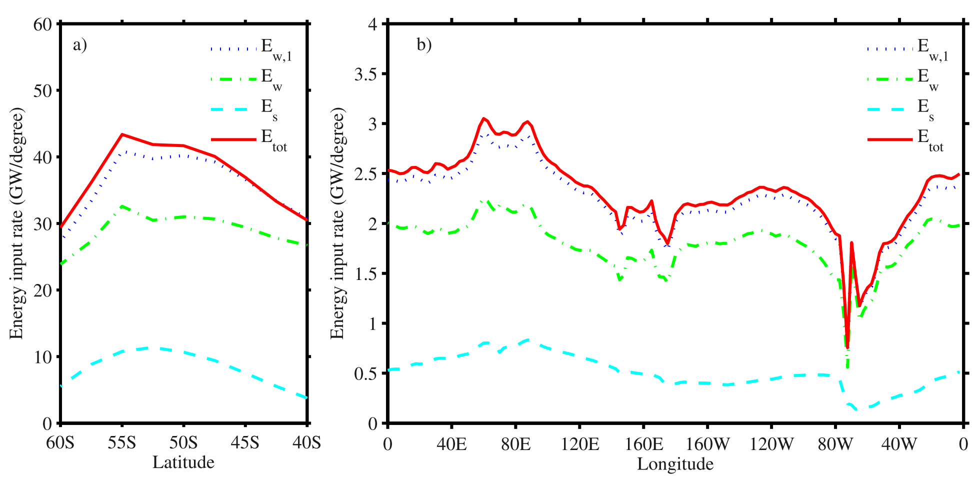

Figure 5. (a) Meridional distributions of $E_{w,1}$, E_w, E_s, and E_{tot} by integrating along longitudes within the ACC. (b) Zonal distributions of $E_{w,1}$, E_w, E_s, and E_{tot} by integrating along latitudes from 40° to 60°S.

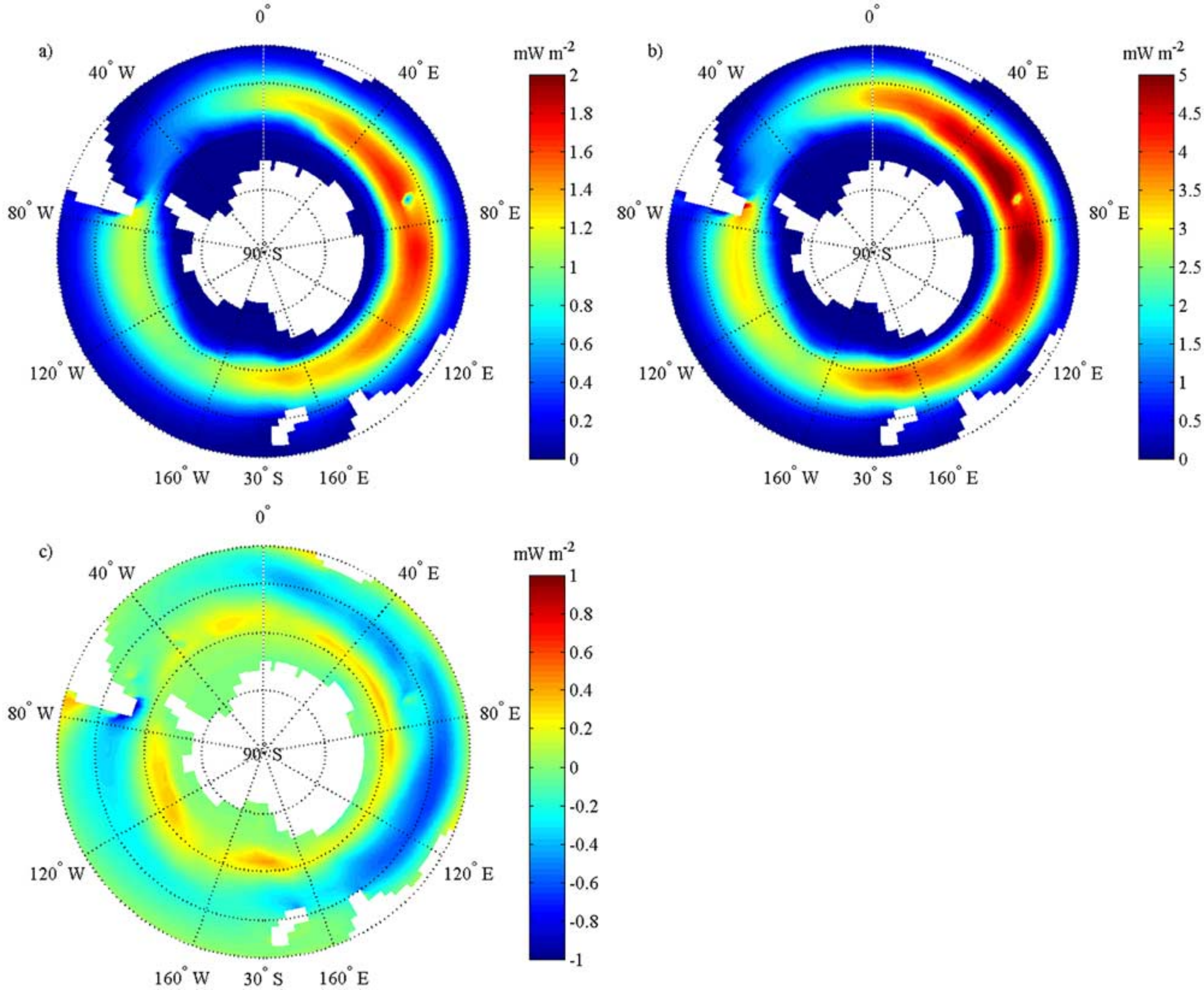

Figure 6. Distributions of the three terms in Stokes drift–induced energy input: (a) $E_{s,1}$, (b) $E_{s,2}$, and (c) $E_{s,3}$.

wind and Stokes drift–induced energy inputs into the Ekman layer, taking into account the wave-induced effects. What we emphasize in the present paper is the wave-added work on the Ekman layer.

[40] The total rate of wind energy input into the Ekman layer contains two components, the direct wind energy input and the Stokes drift–induced energy input. The former is the work rate done by the wind stress acting on the surface Ekman current. Since the profile of the Ekman current is modified when surface waves are added, the direct wind energy input is also influenced by surface waves. The latter is the work done by the Coriolis-Stokes forcing acting on the whole body of water within the Ekman layer. Although this energy input is originally from the wind energy, it is produced through the interaction of the Stokes drift with planetary vorticity. The Stokes drift induced by surface waves not only changes the wind energy input to the Ekman layer but also redistributes the total energy input between the direct wind energy input and Stokes drift–induced energy input.

[41] Using the ECMWF ERA-40 wind stress and surface wave data sets from 1958 to 2001, we estimate that the total

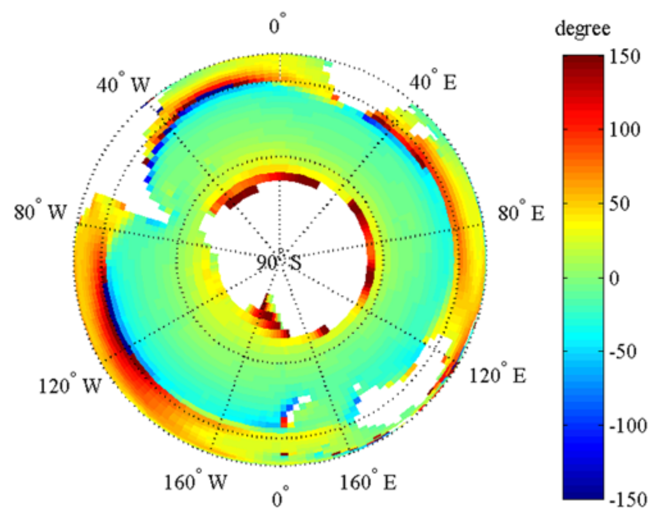

Figure 7. Distribution of the 44-year averaged angles between the wave direction and wind stress direction. The value is positive when the wave direction is to right of the wind stress direction.

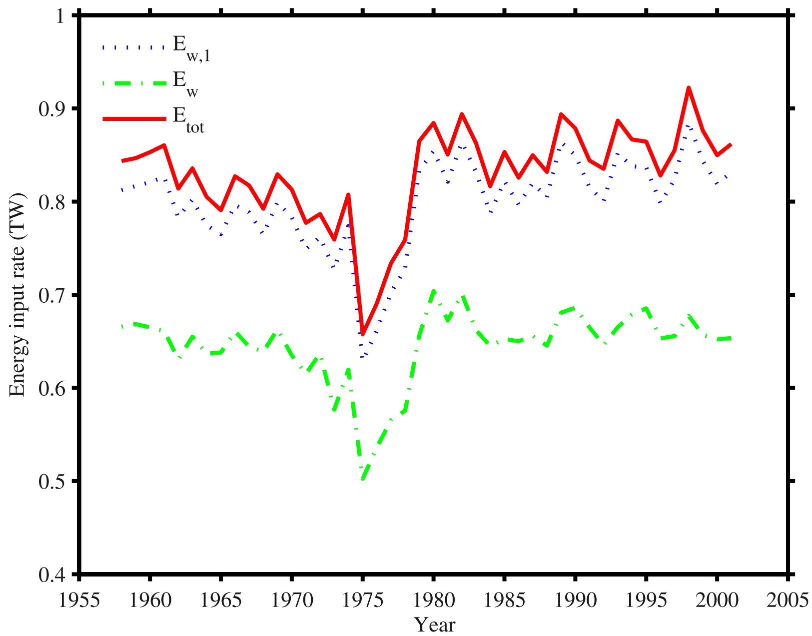

Figure 8. Yearly variations of the wind energy input with wave effects included (E_w, dash-dotted line), wind energy input to the classical Ekman layer ($E_{w,1}$, dashed line), and total wind energy input (E_{tot}, solid line), integrated over the ACC from 1958 to 2001.

rate of energy input to the Ekman-Stokes layer within the ACC is 833 GW, including 650 GW of direct wind energy input (78%) and 183 GW of Stokes drift–induced energy input (22%). Compared to the wind energy input to the classical Ekman layer, the increased mechanical energy input within the ACC is small (about 30 GW). The transferred energy input by the Coriolis-Stokes forcing is 144 GW, which is nearly 18% of the wind energy input to the classical Ekman layer. Nearly 22% of the total mechanical energy input into the Ekman layer within the ACC comes from the wave-induced effects, indicating the importance of waves in driving and maintaining the oceanic general circulation. It also implies that the traditional theory of wind-driven circulations, at least when applied to the ACC, should include the wave-driven effects. Modeling studies are usually performed to examine dynamics and thermodynamics of the ACC by tuning the eddy coefficients and other parameterizations that may compensate for qualitatively or quantitatively incorrect system energetics and other problems. The wave-driven effects are hidden artificially, sometimes incorrectly, in these tuning processes. From the results in this study, we believe that the presence of waves would be effective in improving the ACC modeling.

[42] *Chen et al.* [2002] documented a distribution of the so-called "swell pools" for the global oceans showing that there are three swell-dominated zones located in the eastern tropical and subtropical areas of the Pacific, Atlantic, and Indian ocean basins. Distribution of the angle between the direction of surface waves and that of wind stress is shown to be in agreement with distribution of the swell. That is, a large angle corresponds to a large probability of a swell-dominated zone. The angle effect is expected to have more influence on the wind energy input in the tropical and subtropical oceans. Therefore, this angle effect on the wind energy input should be further examined in specific areas where the swell is dominant.

[43] It should be pointed out that the energy balance in this study obtained from the averaged momentum equation could lead to omission of some terms. The complete energy balance should be derived from the original momentum equation. A critical limitation on the application of this study is that we only used a constant vertical diffusivity to compute the direct wind and Stokes drift–induced energy inputs. Another limitation is that we only considered the deep-ocean condition, neglecting water depth effects, which would definitely influence the wave-current interaction, especially under the shallow-water condition. This study needs, of course, to be improved by using a depth-varying diffusivity and considering limited water depth effects in further studies.

[44] **Acknowledgments.** We thank Wei Wang, Changlong Guan, and Fan Wen for helpful discussions; Ruixin Huang for his encouragement; and ECMWF for supplying the ERA-40 wind stress and surface wave data. We also appreciate the support from the National Basic Research Program of China (2005CB422302, 2005CB422307, and 2007CB411806) and the Great Project of National Natural Science Foundation of China (40490263). This study is partially supported by the U.S. Department of Energy grant (DE-FG02-07ER64448).

References

Alford, M. H. (2003), Improved global maps and 54-year history of wind-work on ocean inertial motions, *Geophys. Res. Lett.*, *30*(8), 1424, doi:10.1029/2002GL016614.

Chen, G., B. Chapron, R. Ezraty, and D. Vandemark (2002), A global view of swell and wind sea climate in the ocean by satellite altimeter and scatterometer, *J. Atmos. Oceanic Technol.*, *19*, 1849–1859, doi:10.1175/1520-0426(2002)019<1849:AGVOSA>2.0.CO;2.

Coleman, G. N., J. H. Ferziger, and P. R. Spalart (1990), A numerical study of the turbulent Ekman layer, *J. Fluid Mech.*, *213*, 313–348, doi:10.1017/S0022112090002348.

Cushman-Roisin, B. (1994), *Introduction to Geophysical Fluid Dynamics*, 320 pp., Prentice-Hall, Englewood Cliffs, N. J.

Hasselmann, K. (1970), Wave-driven inertial oscillations, *Geophys. Fluid Dyn.*, *1*, 463–502.

Huang, N. E. (1979), On surface drift currents in the ocean, *J. Fluid Mech.*, *91*, 191–208, doi:10.1017/S0022112079000112.

Huang, R. X., W. Wang, and L. L. Liu (2006), Decadal variability of wind energy to the world ocean, *Deep Sea Res., Part II*, *53*, 31–41, doi:10.1016/j.dsr2.2005.11.001.

Komen, G. J., L. Cavaleri, M. Donelan, K. Hasselmann, S. Hasselmann, and P. A. E. M. Janssen (1994), *Dynamics and Modelling of Ocean Waves*, 532 pp., Cambridge Univ. Press, Cambridge, U. K.

Lewis, D. M., and S. E. Belcher (2004), Time-dependent, coupled, Ekman boundary layer solutions incorporating Stokes drift, *Dyn. Atmos. Oceans*, *37*, 313–351, doi:10.1016/j.dynatmoce.2003.11.001.

Liu, B., K. J. Wu, and C. L. Guan (2007), Global estimates of wind energy input to subinertial motions in the Ekman-Stokes layer, *J. Oceanogr.*, *63*, 457–466, doi:10.1007/s10872-007-0041-6.

McWilliams, J. C., and J. M. Restrepo (1999), The wave-driven ocean circulation, *J. Phys. Oceanogr.*, *29*, 2523–2540, doi:10.1175/1520-0485(1999)029<2523:TWDOC>2.0.CO;2.

McWilliams, J. C., P. P. Sullivan, and C. H. Moeng (1997), Langmuir turbulence in the ocean, *J. Fluid Mech.*, *334*, 1–30, doi:10.1017/S0022112096004375.

Phillips, O. M. (1977), *The Dynamics of the Upper Ocean*, 336 pp., Cambridge Univ. Press, Cambridge, U. K.

Polton, J. A., D. M. Lewis, and S. E. Belcher (2005), The role of wave-induced Coriolis-Stokes forcing on the wind-driven mixed layer, *J. Phys. Oceanogr.*, *35*, 444–457.

Price, J. F., and M. A. Sundermeyer (1999), Stratified Ekman layers, *J. Geophys. Res.*, *104*, 20,467–20,494, doi:10.1029/1999JC900164.

Rintoul, S. R., C. W. Hughes, and D. Olbers (2001), The Antarctic Circumpolar Current system, in *Ocean Circulation and Climate: Observing and Modelling the Global Ocean*, *Int. Geophys. Ser.*, vol. 77, edited by G. Siedler, J. Church, and J. Gould, pp. 271–302, Academic, San Diego, Calif.

Wang, W., and R. X. Huang (2004a), Wind energy input to the Ekman layer, *J. Phys. Oceanogr.*, *34*, 1267–1275, doi:10.1175/1520-0485(2004)034<1267:WEITTE>2.0.CO;2.

Wang, W., and R. X. Huang (2004b), Wind energy input to the surface waves, *J. Phys. Oceanogr.*, *34*, 1276–1280, doi:10.1175/1520-0485(2004)034<1276:WEITTS>2.0.CO;2.

Watanabe, M., and T. Hibiya (2002), Global estimates of the wind-induced energy flux to inertial motions in the surface mixed layer, *Geophys. Res. Lett.*, *29*(8), 1239, doi:10.1029/2001GL014422.

Weber, J. E. (1983), Steady wind- and wave-induced currents in the upper ocean, *J. Phys. Oceanogr.*, *13*, 524–530, doi:10.1175/1520-0485(1983)013<0524:SWAWIC>2.0.CO;2.

Weber, J. E., and A. Melsom (1993), Volume flux induced by wind and waves in a saturated sea, *J. Geophys. Res.*, *98*, 4739–4745.

Wunsch, C. (1998), The work done by the wind on the oceanic general circulation, *J. Phys. Oceanogr.*, *28*, 2332–2340, doi:10.1175/1520-0485(1998)028<2332:TWDBTW>2.0.CO;2.

Wunsch, C., and R. Ferrari (2004), Vertical mixing, energy, and the general circulation of the oceans, *Annu. Rev. Fluid Mech.*, *36*, 281–314, doi:10.1146/annurev.fluid.36.050802.122121.

Xu, Z. G., and A. J. Bowen (1994), Wave- and wind-driven flow in water of finite depth, *J. Phys. Oceanogr.*, *24*, 1850–1866, doi:10.1175/1520-0485(1994)024<1850:WAWDFI>2.0.CO;2.

B. Liu, Department of Marine, Earth and Atmospheric Sciences, North Carolina State University at Raleigh, Campus Box 8208, Raleigh, NC 27695, USA.

K. Wu, Physical Oceanography Laboratory, Ocean University of China, Qingdao, Shandong 266100, China. (kejianwu@ouc.edu.cn)